• Basic Research •

# Changes in intrinsic excitability of ganglion cells in degenerated retinas of RCS rats

*Yi-Ming Ren, Chuan-Huang Weng, Cong-Jian Zhao, Zheng-Qin Yin*

Southwest Hospital/Southwest Eye Hospital, Third Military Medical University (Army Medical University); Key Lab of Visual Damage and Regeneration & Restoration of Chongqing, Chongqing 400038, China

**Correspondence to:** Cong-Jian Zhao and Zheng-Qin Yin. Southwest Hospital/Southwest Eye Hospital, Third Military Medical University (Army Medical University), Chongqing 400038, China. cj.zhao@yahoo.com; qinzyin@aliyun.com

Received: 2018-02-04 Accepted: 2018-03-16

## Abstract

**• AIM: To evaluate the intrinsic excitability of retinal ganglion cells (RGCs) in degenerated retinas.**

**• METHODS: The intrinsic excitability of various morphologically defined RGC types using a combination of patch-clamp recording and the Lucifer yellow tracer in retinal whole-mount preparations harvested from Royal College of Surgeons (RCS) rats, a common retinitis pigmentosa (RP) model, in a relatively late stage of retinal degeneration (P90) were investigated. Several parameters of RGC morphologies and action potentials (APs) were measured and compared to those of non-dystrophic control rats, including dendritic stratification, dendritic field diameter, peak amplitude, half width, resting membrane potential, AP threshold, depolarization to threshold, and firing rates.**

**• RESULTS: Compared with non-dystrophic control RGCs, more depolarizations were required to reach the AP threshold in RCS RGCs with low spontaneous spike rates and in RCS OFF cells (especially A2o cells), and RCS RGCs maintained their dendritic morphologies, resting membrane potentials and capabilities to generate APs.**

**• CONCLUSION: RGCs are relatively well preserved morphologically and functionally, and some cells are more susceptible to decreased excitability during retinal degeneration. These findings provide valuable considerations for optimizing RP therapeutic strategies.**

**• KEYWORDS:** retinal degeneration; ganglion cell; intrinsic excitability; patch clamp

**DOI:10.18240/ijo.2018.05.07**

**Citation:** Ren YM, Weng CH, Zhao CJ, Yin ZQ. Changes in intrinsic excitability of ganglion cells in degenerated retinas of RCS rats. *Int J Ophthalmol* 2018;11(5):756-765

## INTRODUCTION

Retinal ganglion cells (RGCs) integrate visual information from photoreceptors *via* parallel synaptic pathways and encode the result as action potentials (APs) that are sent to higher visual centres[1]. The AP encoding efficiency in RGCs is largely determined by the various intrinsic physiological properties of 15-20 different morphological types of RGCs[1-2]. As the only retinal projection neurons, RGCs form the biological substrate for visually repairing various pathologies, such as retinitis pigmentosa (RP). RP is a heterogeneous group of inherited diseases in which photoreceptor death is usually followed by the morphological and functional remodelling of downstream circuitry[3-4]. Several vision rescue strategies for RP use RGC population as a direct target. Light is transformed into electric signals by either epiretinal electronic prostheses[5-7] or light-sensitive proteins in RGCs *via* optogenetic tools[8-10]. The effectiveness of these electrical signals is largely dependent on the intrinsic excitability of the RGCs. However, the impact of photoreceptor loss on the intrinsic excitability of RGCs is not fully understood.

Previous studies on RGC intrinsic electrophysiological changes in degenerated retinas have mainly focused on spontaneous rhythmic activities in RGCs[11-15] or were performed on retinal slices in which the RGC dendrites were largely destroyed[16]. Other studies on RGC excitability levels were based on epiretinal or subretinal extracellular electric stimulation, and elevated stimulation thresholds in degenerated retinas were widely observed[17-21]. However, these results may have been influenced by numerous factors, including the remodelled retinal circuitry[19,22], the RGC density[18,23], the relative position of the RGC to the stimulating electrode[23] and the intrinsic RGC excitability, and most of these experiments did not consider an individual cell's morphological type. Hence, we aimed to elucidate whether decreased intrinsic excitability exists in various types of RGCs in degenerated retinas.

In the present study, we utilized the Royal College of Surgeons (RCS) rat model mimicking a type of human RP disease triggered by phagocytosis defect in retinal pigmented epithelium cells[24]. Photoreceptors are almost completely absent at P90 in this model[25]. In this late stage of retinal degeneration, the intrinsic physiological properties of various morphologically defined RGC types were recorded using a

combination of whole-cell patch-clamp recording and the Lucifer yellow tracer in retinal whole-mount preparations. Compared with control RGCs, more depolarizations were required to reach the AP threshold in some RCS RGCs, while all recorded RGCs could generate APs.

## MATERIALS AND METHODS

**Animals** All animal experiments were approved by the Laboratory Animal Welfare and Ethics Committee of the Third Military Medical University and were carried out in accordance with the Association for Research in Vision and Ophthalmology (ARVO) Statement for the Use of Animals in Ophthalmic and Vision Research. RCS-$p^+$ rats (dystrophic, abbreviated as RCS, P91-P97, *n*=25) and RCS-rdy$^+$p$^+$ rats (non-dystrophic, abbreviated as control or "Ctrl", P30-P97, *n*=29) were employed in the experiments. All animals (both males and females) were provided by the Experimental Animal Department of Third Military Medical University and were housed at a constant temperature in a 12-h light/dark cycle.

**Retinal Whole-mount Preparations** The rats were dark-adapted for at least 2h, anesthetized with sodium pentobarbital (100 mg/kg, i.p.) and then sacrificed by cervical dislocation. Their eyes were quickly enucleated and bathed in a carbogenated (95% $O_2$/5% $CO_2$) extracellular solution comprising 124 mmol/L NaCl, 2.8 mmol/L KCl, 2 mmol/L $CaCl_2$, 2 mmol/L $MgSO_4$, 1.25 mmol/L $NaH_2PO_4$, 26 mmol/L $NaHCO_3$, 10 mmol/L D-glucose, and 0.4 mmol/L sodium ascorbate (pH 7.4). Under red light illumination, the cornea, iris and lens were removed, the retina was gently peeled from the eyecup, and the vitreous body was removed with forceps. Then, each retina was typically divided into 4 pieces, and the pieces were bathed in the carbogenated extracellular solution in the dark. One retinal piece was transferred into a recording chamber with ganglion cell layer (GCL) up and fixed with a small grid. The chamber was perfused with the carbogenated extracellular solution described above at 25℃-26℃ in very dim light (about 0.1 lx). The retina could be visualized clearly under differential interference contrast (DIC) optics by infrared illumination using a complementary metal-oxide semiconductor (CMOS) camera (Andor Zyla 4.2, Andor Technology Ltd., Belfast, UK) attached to an upright fluorescence microscope (BX51WI, Olympus Optical, Tokyo, Japan) equipped with a 40× water immersion lens.

**Whole-cell Patch-clamp Recording** To obtain a whole-cell patch-clamp recording, we first used a glass pipette pulled on a P97 puller (Sutter Instrument, Novato, CA, USA) to tear a small hole in the inner limiting membrane to expose the cell bodies. Clean pipettes ranging from 3-7 MΩ filled with intracellular solution were used to patch the exposed cells that had smooth surfaces. The intracellular solution comprised 112.5 mmol/L $CsCH_3SO_3$, 9.7 mmol/L KCl, 1 mmol/L $MgCl_2$, 1.5 mmol/L EGTA, 10 mmol/L HEPES, 4 mmol/L $ATPMg_2$, 0.5 mmol/L $GTPNa_3$, and 1% Lucifer yellow (pH 7.3). All extracellular and intracellular solution chemicals were obtained from Sigma-Aldrich. Patch-clamp recordings were performed with a Multiclamp 700B amplifier (Molecular Devices, Sunnyvale, CA, USA). Signals were low-pass filtered at 3 kHz and sampled at 20 kHz with a 1550A analog-to-digital converter (Molecular Devices, Sunnyvale, CA, USA).

**Physiological Data Collection** After formation of a high-resistance (>1 GΩ) seal, a brief amount of negative pressure was applied to obtain the whole-cell mode, and the recording began after 3min. Series resistance ($R_s$), membrane resistance ($R_m$) and membrane capacitance ($C_m$) data from pCLAMP membrane tests were acquired by averaging 30-50 measurements in response to 5 mV pulses. The average $R_s$ was 25.5±0.6 MΩ (range, 11-41 MΩ; *n*=117). To elicit APs, a series of depolarizing current steps at the 40 pA delta level were injected for 800ms. Resting membrane potentials (RMPs) were not corrected for liquid junction potentials. Peak amplitudes and AP half widths were quantified using MiniAnalysis software (Synaptosoft, Leonia, NJ, USA). Action potential thresholds (APTs) were measured using Igor software (WaveMetrics, Lake Oswego, OR, USA) and defined as the membrane potential when the voltage deflection exceeded 20 mV/ms[26]. Most data represent the average of 10 such measurements.

**Morphological Data Collection** Following whole-cell recording for approximately 10min, Lucifer yellow should have fully diffused to the dendrites. Fluorescence images of the dendrites were obtained at 2 μm intervals using a 40× water immersion lens under a 470 nm LED (M470L3, Thorlabs, Newton, NJ, USA). The presence of an axon was used to distinguish RGCs from displaced amacrine cells. Inner plexiform layer (IPL) borders were defined by cell soma positions of the inner nuclear layer (INL) and the GCL visualized under differential interference contrast (DIC) optics[27-28]. Thus, RGC dendritic stratifications relative to the proximal (0) and distal IPL margins (100%) were measured (Figure 1A). For RGCs with a large dendritic field, we typically spliced four images from each quadrant into a complete dendritic image using Adobe Photoshop (USA). To measure the dendritic field diameter, a polygon was drawn by linking the dendritic tips using Image J programme (NIH, Bethesda, MD, USA), and the area was calculated and converted back to the diameter by assuming a circular dendritic field[2,29]. Similarly, to determine soma size, a freehand line was drawn around the borders of the cell body to calculate the soma diameter.

**Estimating the Precision of Dendritic Stratification** For estimating the precision of the RGC dendritic stratification from the recorded DIC fluorescence images, some retinal whole-mounts were fixed in 4% paraformaldehyde (PFA) and then incubated with 4',6-diamidino-2-phenylindole (DAPI). Z-stack images of RGC dendrites were acquired at 0.5-0.6 μm

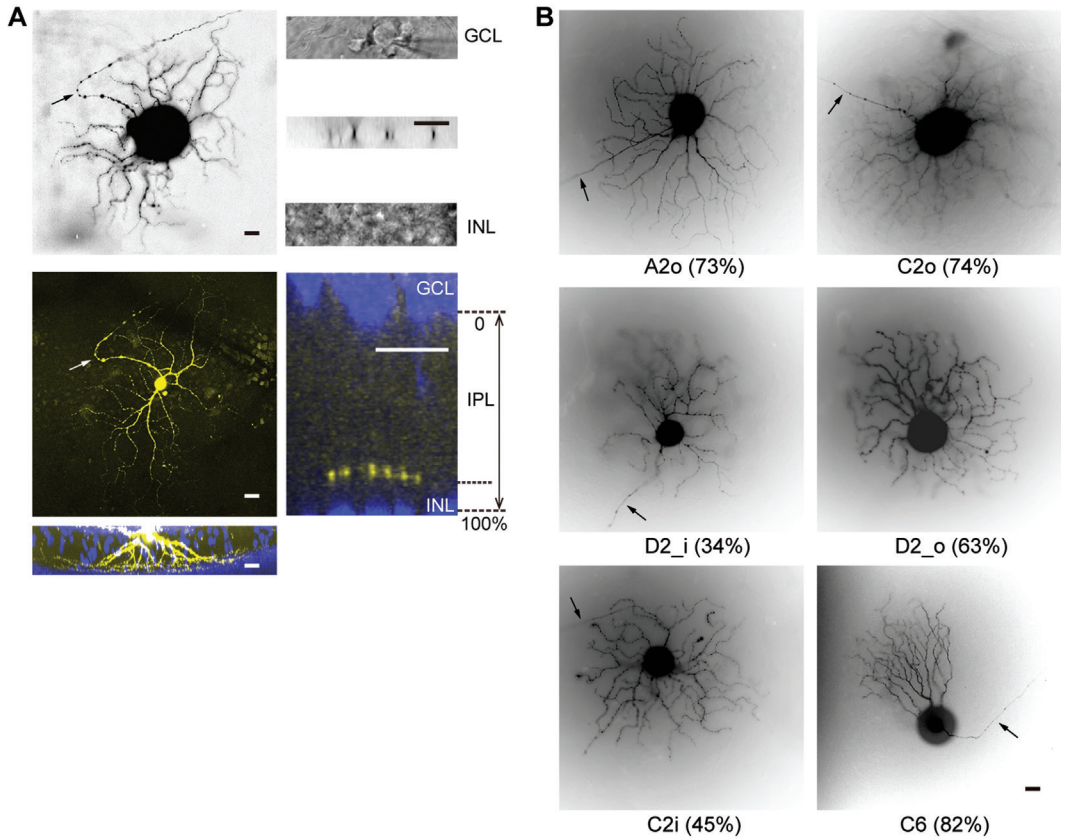


**Figure 1 Identification of RGCs** A: Stacked fluorescence image of a RGC stained with Lucifer yellow (monochrome image). RGCs were identified by the presence of an axon (arrows). The GCL and INL somas were visualized under infrared DIC optics to estimate the IPL borders. The concatenate z-stack image shows the position of the RGC dendrites. An image of the same cell as reconstructed by confocal microscopy. Cell nuclei stained with DAPI were used to accurately calculate the dendritic stratification. The precision of dendritic stratification using DIC fluorescent imaging was estimated to be approximately 6% compared with that using confocal or two-photon imaging ($n$=8); B: Stacked fluorescence images of several types of RGCs stained with Lucifer yellow. The numbers in parentheses indicate the average dendritic stratifications in control rats. Note that C6 cells have been reported in only mice and not in rats in previous studies. All scale bars: 20 μm.

intervals using a confocal microscope or a custom-built two-photon imaging system. DAPI-stained nuclei defined the IPL borders. Compared with confocal and two-photon images, the precision of dendritic stratification according to DIC fluorescent images was approximately ±6% ($n$=8; Figure 1A), which was enough for the morphological classification for RGCs.

**Light Stimuli** To further determine the centre sign of RGC's receptive field, light stimuli were applied using a 470 nm LED, which was controlled by an LED driver and Master-8 (A.M.P. Instruments, Jerusalem, Israel). Stimuli were then delivered to the retina *via* the microscope port. The intensity of the initial LED light was about 230 lx. Light stimuli were usually applied 3 times for a duration of 0.5s each at 4s intervals.

**Data Sources** For analyses of APs evoked by depolarizing currents, low-quality cells, defined as cells with marked RMP instability or cells whose AP did not exceed 0 mV, were excluded. In addition, cells without spontaneous spikes were also excluded from the APT, RMP, and $R_m$ analyses. All these data were used to analyse the morphological properties of various cell types. Because no significant differences were observed in any of the morphological or physiological properties (dendritic stratification, dendritic field diameter, AP peak amplitude, AP half width, RMP, APT, APT-RMP, maximal firing frequency, mean firing frequency) in control rats among various ages (P30-P34, $n$=12; P44-P48, $n$=7; and P90-P97, $n$=10), therefore all control samples from P30-P97 were pooled as reference to compare the RCS groups.

**Statistical Analysis** Data are presented as the mean±SEM. Statistical analyses were performed using IBM SPSS Statistics (V.20, USA). Student's $t$-tests were used for comparisons between two groups (*e.g.* control versus RCS, "high-rate" group versus "low-rate" group in control rat). One-way ANOVAs were used to assess statistical significance among ON, OFF and ON-OFF cells.

## RESULTS

**Morphological Stability of RGCs in RCS Retinas** We recorded the morphological properties of 117 rat RGCs, including 65 control cells (P30-P97) and 52 RCS cells (P91-P97). As previously described by Sun *et al*[29], rat RGCs are initially classified into groups A, B, C, D and then divided into 16 different types based on their soma size, dendritic

field diameter, dendritic structure and dendritic stratification. Fourteen of 16 RGC types were encountered in this study. Additionally, one more RGC type, C6 cell ($n$=3, 2 control and 1 RCS) (Figure 1B), which has been identified in mouse retinas but not in rat retinas, was recorded[29-30]. C6 cell has been defined as having all dendrites extending in one direction and stratifying in only the outer IPL. Consistent with previous measurements[2], type A cells had the largest dendritic field diameter (398±10 μm; $n$=30 Ctrl), while type B cells had the smallest (196±19 μm; $n$=4 Ctrl).

To evaluate the effects of photoreceptor death on RGC morphological characteristics, the dendritic field diameter and stratification were measured and compared in RCS and control retinas of the major types of RGCs in this study, including A2 outer (A2o), C2 outer (C2o), C2 inner (C2i), and D2 (D2_i and D2_o indicate the inner and outer dendritic arbors, respectively; Figure 1B). The dendritic stratifications across all these RGC types were not significantly different between RCS and control retinas (Figure 2A; A2o: $P$=0.320, 20 Ctrl, 9 RCS; C2o: $P$=0.568, 7 Ctrl, 10 RCS; C2i: $P$=0.476, 4 Ctrl, 6 RCS; D2_o: $P$=0.103, 8 Ctrl, 9 RCS; D2_i: $P$=0.071, 8 Ctrl, 9 RCS); their dendritic field diameters were also not significantly different (Figure 2B; $P$=0.079, 0.128, 0.890, 0.065, and 0.567 for A2o, C2o, C2i, D2_o, and D2_i, respectively). These results suggest that the dendritic morphologies of RGCs remain relatively stable in the P90 stage in RCS retinas. No significant differences in dendritic stratification or dendritic field diameter in any RGC type were observed between control and RCS rats. The sample sizes for this figure and all subsequent figures are indicated at the bottom of each bar unless otherwise specified. The whiskers in Figure 2A indicate minimal and maximal values. The error bars in Figure 2B and in all subsequent figures indicate SEM unless otherwise specified.

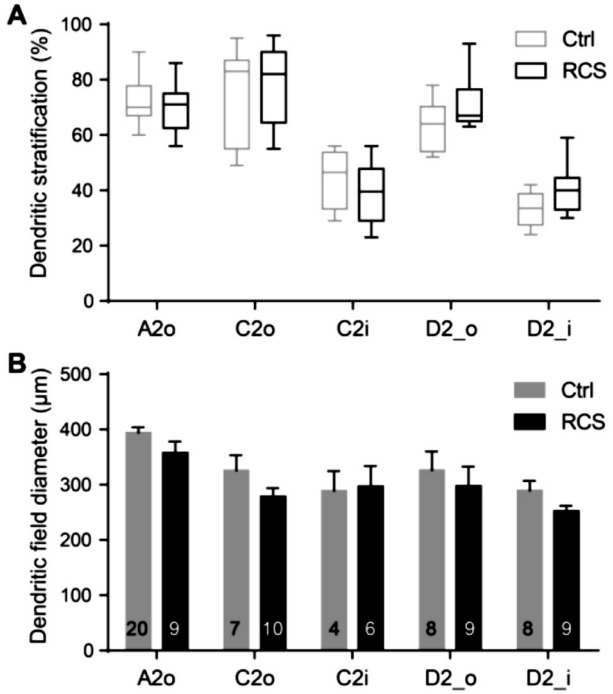


**Figure 2 RGC dendritic stratifications and field diameters in control and RCS retinas** Comparisons of RGC dendritic stratifications (A) and dendritic field diameters (B) between control and RCS rats.

**RCS RGCs Retain the Capability to Generate Spikes** APs are the basic unit of visual information transmission in RGCs[1]. We next wanted to address whether some RGCs lose their capability to generate APs during retinal degeneration. In the present study, 98.1% of the control RGCs and 94.7% of the RCS RGCs fired spikes spontaneously, and all the other cells could generate APs resulting from 40 to 160 pA depolarizing currents (Figure 3A, 3B). Notably, all of the low-quality cells could also generate APs (see Methods part). These data demonstrate that the spiking capability in RCS RGCs of a relatively late retinal degeneration stage (P90) is largely preserved. To further assess the capabilities of RGCs to generate APs, the intrinsic excitability properties of each RGC, including their peak amplitude, AP half width, RMP, APT, and APT-RMP value, were measured. The average values were 67.2±1.1 mV, 3.9±0.3ms, -50.6±0.3 mV, -42.0±0.6 mV, and 8.6±0.5 mV, respectively, for control cells ($n$=51) and 64.5±1.7 mV, 3.2±0.3ms, -50.2±0.6 mV, -40.5±0.6 mV, 9.7±0.5 mV, respectively, for

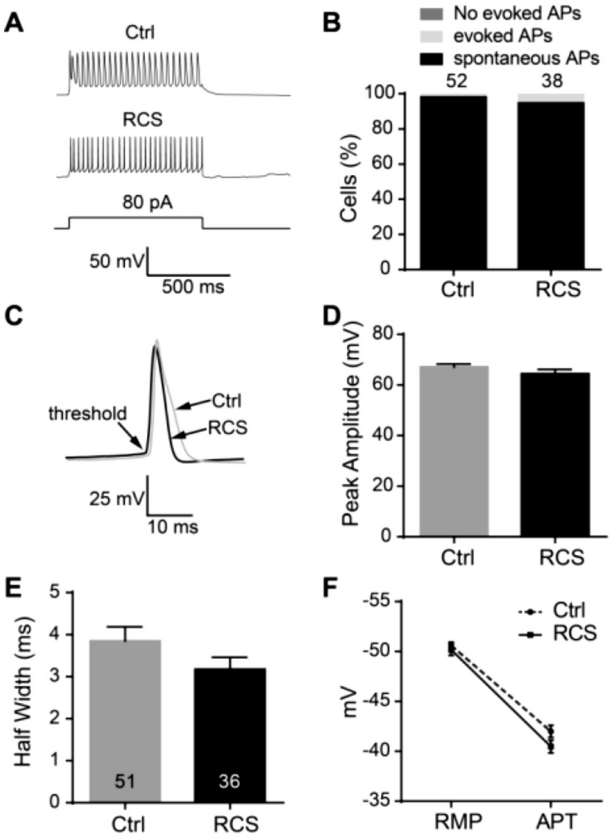


**Figure 3 Retaining the capability to generate spikes in RCS RGCs at P90 and combined intrinsic property data** A: Representative recording traces in response to depolarizing current injections; B: All RGCs in both control and RCS rats were capable of spiking spontaneously or in response to the injection of depolarizing currents at 40 to 160 pA. The sample sizes are indicated at the top of each bar; C: Representative recording traces of spontaneous APs; D-F: The peak amplitude, AP half width, RMP, APT and the APT-RMP value were not significantly different between control and RCS rats.

RCS cells ($n$=36). Further analyses revealed no significant differences between control and RCS cells for all these parameters (Figure 3C-3F; $P$=0.175, 0.149, 0.520, 0.095, 0.157 for peak amplitude, half width, RMP, APT, and APT -RMP value, respectively). However, altered trends were observed for the half width and APT values. The sample sizes for Figure 3D-3F are indicated at the bottom of each bar in Figure 3E. Note that the sample sizes here are less than those in Figure 3B because RGCs without spontaneous spikes were rejected.

**Decreased Intrinsic Excitability of Some RCS RGCs**

To carefully analyse the intrinsic excitability properties, we categorized these data by spontaneous spike rates and morphological characteristics, since the spike rate is closely related to cellular excitability[31] and different morphologically identified RGC types have distinct patterns of intrinsic physiological properties[2,32]. In the present study, cells with spontaneous AP (sAP) frequencies greater than 10 Hz were classified as "high-rate" cells (Ctrl, $n$=10; RCS, $n$=12), while the remaining cells were classified as "low-rate" cells (Ctrl, $n$=42; RCS, $n$=24). Additionally, we categorized each RGC type as ON, OFF, or ON-OFF based mainly on their dendritic stratification and partially on their light responsiveness because light responses were abolished or very weak in some RCS RGCs. Consistent with previous reports[32-33], dendrites in most ON cells stratified in the inner IPL (0-60% depth), while those in OFF cells stratified in the outer IPL (60%-100% depth), and those in ON-OFF cells stratified in both sublaminae (Figure 2A).

Comparisons of peak amplitudes and AP half widths between control and RCS RGCs in the rate and morphological groups are shown in Figure 4. Note that data from the three morphological groups were from only low-rate cells (Ctrl: $n$=16, 19, 6; RCS: $n$=8, 9, 7 for ON, OFF and ON-OFF cells, respectively); and due to the number of high-rate cells was small, statistical analysis did not involve three morphological groups with high firing frequency. Significant differences in peak amplitude were observed between only the two rate groups in the control cells ($P$=0.014), as no significant differences were found in RCS cells between the two rate groups ($P$=0.163) nor in the other groups between control and RCS rats (low rate: $P$=0.316; high rate: $P$=0.883; ON: $P$=0.255; OFF: $P$=0.357; ON-OFF: $P$=0.858). No significant differences in peak amplitude among ON, OFF and ON-OFF cells were observed in control or RCS retinas (Ctrl: $P$=0.297; RCS: $P$=0.313).

Compared with half widths in each control group (Figure 4B1-4B2), those in all the RCS groups were slightly but not significantly shorter (low rate: $P$=0.177; high rate: $P$=0.756; ON: $P$=0.353; OFF: $P$=0.779; ON-OFF: $P$=0.075). No significant differences were observed between the two rate groups (Ctrl: $P$=0.576; RCS: $P$=0.868). No significant differences in half width among the ON, OFF and ON-OFF

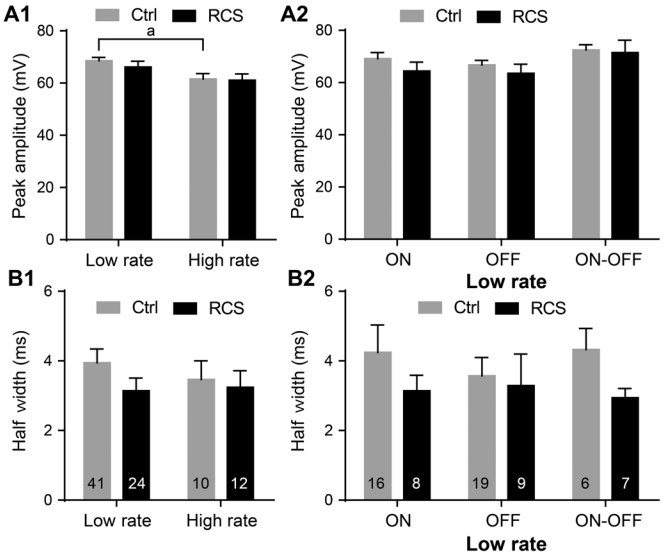


**Figure 4 Peak amplitudes and AP half widths in control and RCS RGCs** A1-A2: Comparable peak amplitudes between control and RCS rats in two rate groups and three morphological groups. Differences were significant between only the two rate groups of control RGCs ($^aP$<0.05). Low rate: sAP≤10 Hz; high rate: sAP>10 Hz; B1-B2: No significant differences in half width between control and RCS cells were observed in any of the five groups.

cells were observed in control or RCS retinas (Ctrl: $P$=0.692; RCS: $P$=0.932).

To evaluate which group of RCS RGCs required more depolarizations to reach the APT compared to the control, statistical analyses were performed on RMP, APT and APT-RMP values (Figure 5). Compared with the RMPs in control cells, RMPs in RCS cells were relatively constant in all five groups (low rate: $P$=0.755; high rate: $P$=0.342; ON: $P$=0.908; OFF: $P$=0.321; ON-OFF: $P$=0.779). RCS cells with high spike rates were significantly more depolarized than those with low spike rates ($P$=0.022), while no significant differences were found in control cells between the two rate groups ($P$=0.119). No significant differences in RMP among the ON, OFF and ON-OFF cells were observed in control or RCS retinas (Ctrl: $P$=0.329; RCS: $P$=0.394).

Regarding APT values (Figure 5B1, 5B2), no significant differences were observed between control and RCS cells in any of the five groups (low rate: $P$=0.137; high rate: $P$=0.501; ON: $P$=0.284; OFF: $P$=0.173; ON-OFF: $P$=0.406); however, except for the ON-OFF group, the absolute RCS APT values in all of the other groups were weakly decreased by 1.1-2.8 mV. No significant differences in APT value were observed between the two rate groups (Ctrl: $P$=0.865; RCS: $P$=0.870) or among the ON, OFF and ON-OFF cells (Ctrl: $P$=0.351; RCS: $P$=0.694).

The APT-RMP values in low-rate RCS cells were not only higher than those in low-rate control cells (by 1.9 mV; $P$=0.042) but also higher than those in high-rate RCS cells (by 2.9 mV; $P$=0.004), and a significant increase was also observed in the RCS OFF cell group compared to the control OFF cell

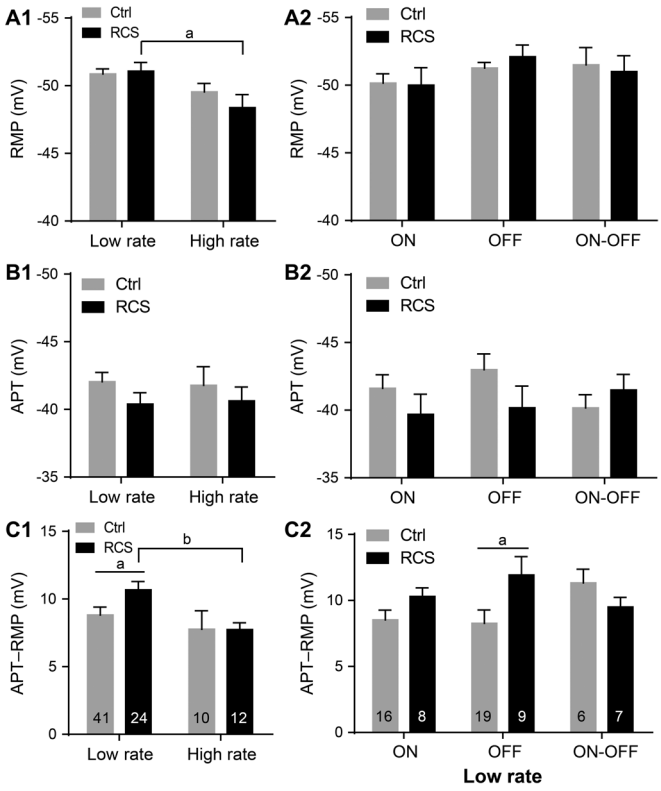


**Figure 5 Larger depolarizations were required to reach APTs in some RCS RGCs compared to control RGCs** A1-A2: Comparable range of RMPs between control and RCS rats in two rate groups and three morphological groups. The RMPs were significantly more depolarized in RCS cells with high spike rates compared to those with low spike rates ($^aP$<0.05); B1-B2: No significant differences in APT between control and RCS cells were observed in any of the five groups; C1-C2: The APT-RMP values of low-rate RCS cells were not only significantly higher than those of low-rate control cells but was also higher than those of high-rate RCS cells, and the APT-RMP values of RCS OFF cells were significantly higher than those of control OFF cells ($^aP$<0.05, $^bP$<0.01).

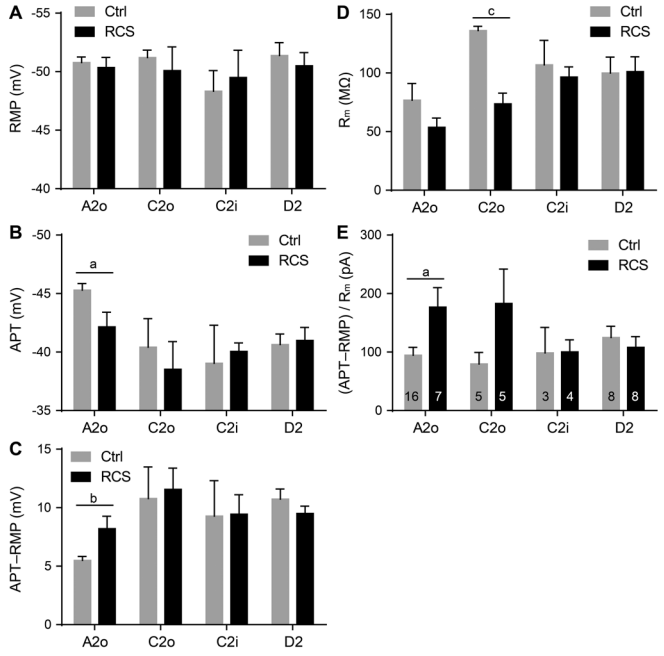


**Figure 6 Some OFF cells required more currents to reach the APTs in RCS retinas than in control retinas** A: No significant differences between control and RCS RMPs were observed in any of the four types of RGCs; B: A significant difference in APT was observed between only control and RCS A2o cells ($^aP$<0.05); C: A significant difference in the APT-RMP value was observed between only control and RCS A2o cells ($^bP$<0.01); D: A significant difference in $R_m$ was observed between only control and RCS C2o cells ($^cP$<0.001); E: A significant difference in the (APT-RMP)/$R_m$ value was observed between only control and RCS A2o cells ($^aP$<0.05).

group (by 3.8 mV; $P$=0.047). No significant differences were observed in the other groups between control and RCS rats (high rate: $P$=0.989; ON: $P$=0.136; ON-OFF: $P$=0.168) or in control rats between the two rate groups ($P$=0.443). No significant differences among the ON, OFF and ON-OFF cells were observed (Ctrl: $P$=0.207; RCS: $P$=0.262).

The amount of current required to reach the APT is not only determined by voltage but also by the $R_m$. Because the $R_m$ values of different RGC types vary extensively, we further analysed these values in the major cells, including the A2o, C2o, C2i and D2 types (Figure 6; Ctrl: $n$=16, 5, 3, and 8; RCS: $n$=7, 5, 4, and 8, for A2o, C2o, C2i, and D2 cells respectively). Consistent with previous reports[2], A2o cells had the lowest $R_m$ (77±14 MΩ for control cells). No significant differences in RMP between the RCS and control groups were observed in these RGC types ($P$=0.646, 0.626, 0.724, and 0.589 for A2o, C2o, C2i, and D2, respectively). Significant differences in APT ($P$=0.015, 0.595, 0.738, and 0.813 for A2o, C2o, C2i, and D2, respectively) and the APT-RMP value ($P$=0.004, 0.815, 0.962, 0.273 for A2o, C2o, C2i and D2, respectively) were observed in only A2o cells. The $R_m$ values were significantly decreased in RCS C2o cells compared to control C2o cells ($P$=0.315, <0.001, 0.629, and 0.949 for A2o, C2o, C2i, and D2, respectively). We next calculated the current required to reach the APT by Ohm's law: I=(APT-RMP)/$R_m$. A2o cells in RCS rats required more current to generate an AP than control cells ($P$=0.012), and another type of OFF cells (C2o) showed a similar but non-significant tendency ($P$=0.134); C2i and D2 cells were stable between control and RCS rats (C2i: $P$=0.972; D2: $P$=0.543).

**Decreased Maximal Firing Frequency in RCS RGCs with Low Spontaneous Spike Rates** To further verify the decreased intrinsic excitability in RCS RGCs with low spontaneous spike rates compared to the control, AP firing frequencies elicited by depolarizing currents (0 pA, 40 pA and 80 pA) were measured and categorized into "high-rate" (sAP>10 Hz) and "low-rate" (sAP≤10 Hz) groups. In addition, only cells with sustained firing patterns at 80 pA were included. According to previous reports, firing patterns include single, phasic (or transient), adapting, sustained and irregular patterns[28,34-35]. In this study, most RGCs in both control and RCS rats exhibited the

sustained pattern; while 2 of 42 control cells and 3 of 26 RCS cells exhibited the adapting pattern, and 4 of 42 control cells and 2 of 26 RCS cells exhibited the irregular pattern.

In Figure 7, "mean frequency" represents number of spikes per second during an 800-ms pulse. "Maximal frequency" represents the maximal value of the mean frequency and the inverse of the time between the first two APs during a depolarizing pulse. The maximal instantaneous frequency determines the synaptic transmission fidelity and the dynamic signalling range[36].

Comparable spontaneous mean frequencies (0 pA group) between control and RCS cells were observed in both the low- and high-rate groups (low rate: $P$=0.359; high rate: $P$=0.893). Although no significant differences in the mean frequencies at 40 pA and 80 pA between control and RCS cells were observed in either group (low rate: $P$=0.054 for 40 pA, $P$=0.462 for 80 pA; high rate: $P$=0.288 for 40 pA, $P$=0.157 for 80 pA), the RCS curve was below the control curve in the low-rate group, while the RCS curve was above the control curve in the high-rate group (Figure 7A1-7A2). The maximal frequencies in RCS cells were significantly lower than those in control cells in the low-rate group (40 pA: $P$=0.009; 80 pA: $P$=0.005), while no significant differences were observed in the high-rate group (40 pA: $P$=0.327; 80 pA: $P$=0.272), which could be explained by elevated depolarization of the RMP toward the APT in RCS cells of the low-rate group, as mentioned above (Figure 5C1).

The ratios of mean to maximal firing frequency between control and RCS cells were not significantly different between the two groups (low rate: $P$=0.456 for 40 pA, $P$=0.179 for 80 pA; high rate: $P$=0.540 for 40 pA, $P$=0.822 for 80 pA), while this ratio in the low-rate group was significantly lower than that in the high-rate group for control cells at 80 pA (Ctrl: $P$=0.093 for 40 pA, $P$=0.015 for 80 pA; RCS: $P$=0.540 for 40 pA, $P$=0.153 for 80 pA), which could be explained by the fact that RGCs with low spontaneous spike rates were more likely to produce a higher first instantaneous frequency (Figure 7B1, 7B2; $P$=0.003 for Ctrl 80 pA). Similar analyses of the mean frequencies, maximal frequencies and ratios of the mean to maximal frequencies were performed in ON, OFF and ON-OFF cells, revealing no significant differences in any of the groups between control and RCS rats (data not shown).

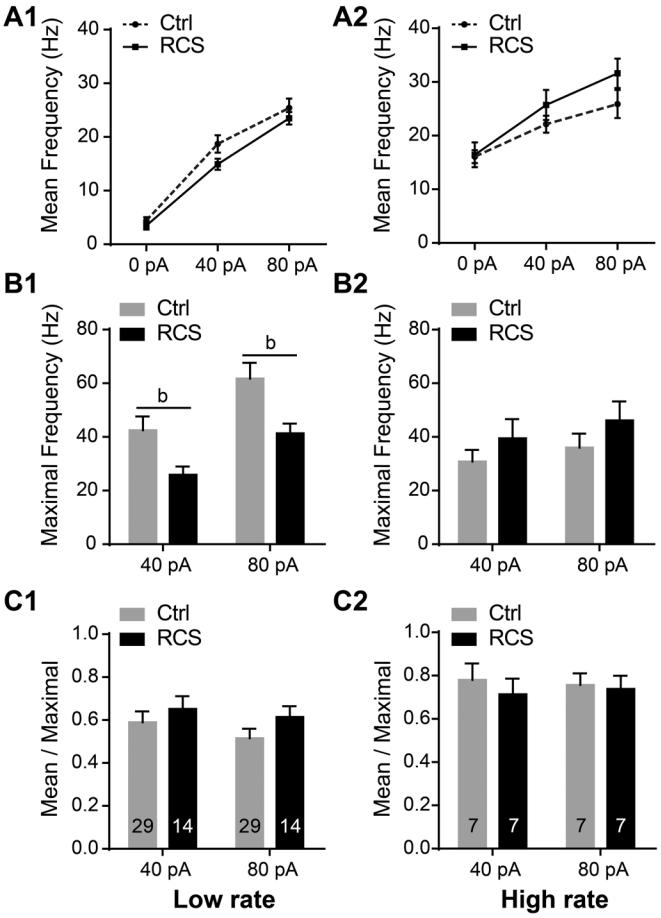


**Figure 7 Decreased maximal firing frequency in RCS cells with low spontaneous spike rates** A1-A2: Curves between the injected currents and mean frequencies of evoked spikes in the low- and high-rate groups. No significant differences between control and RCS cells at any injection current were observed in either group. B1-B2: The maximal frequencies of RCS cells were significantly decreased compared to those of control cells in the low-rate group at both the 40 pA and 80 pA depolarization steps ($^bP$<0.01). C1-C2: No significant differences in the ratio of mean to maximal firing frequency were observed between control and RCS RGCs in either rate group.

## DISCUSSION

Our results showed that all recorded RGCs retain their ability to elicit APs, that RCS RGCs in the late stages of retinal degeneration exhibit relatively stable dendritic morphologies, and that the levels of intrinsic excitability decrease in some RCS RGCs, including cells with low spontaneous spike rates and OFF cells. These findings represent detailed intrinsic excitability measurements from identified RGC types and provide implications for vision rescue strategies.

Sun *et al*[29-30]. reported that the morphological classifications of mouse and rat RGCs were nearly identical, except for the C5 and C6 types, which were found in only mouse retinas. To our knowledge, these data have not been reported in other rat studies. Fortunately, we encountered C6 cells in rat retinas, which could be explained by the high degree of homology between mice and rats. C6 RGCs are easily identifiable because all their dendrites extend in one direction and stratify in the outer OPL. Further studies in mice demonstrated that C6 cells express the marker junctional adhesion molecule B (JAM-B) and respond to upward motion[37].

RGCs are the only output neurons of the retina, and multiple therapeutic approaches for RP rely on the preservation of their morphology and function. Regarding dendritic morphology, several recent studies have shown that RGCs survive and maintain stable dendritic morphology during late stages of degeneration at 6-11 months of age in rd1 or rd10

mice[38-40]. These two RP models carry mutations in the gene encoding rod-specific phosphodiesterase[41-42]. However, RGC morphological research is rare in RCS rats, a classical animal model of debris-initiated retinal degeneration triggered by a phagocytosis defect in retinal pigmented epithelium cells[24]. Photoreceptor degeneration becomes evident at P20; at P90, only a few residual cone pedicles are evident, and the scotopic b-wave is undetectable. Correspondingly, second-order neurons in RCS retinas are rapidly remodelled, especially the atrophy and sprouting of bipolar and horizontal cell dendrites[25]. Previous studies on the numbers of RGCs have found no difference between control and RCS retinas at P180[43-44]. In our study, RGC dendrites were stained with Lucifer yellow during electrical activity recordings. Morphological analyses revealed that the four major types of RGCs encountered (A2o, C2o, C2i, and D2) maintained their dendritic stratifications and dendritic field sizes at P90. We did not investigate older rats due to difficulties with removing a very thin retina and maintaining sufficient vitality for patch-clamp recordings. Together, our results support the previous conclusion that RGC morphologies are resistant to photoreceptor loss during retinal degeneration.

The level of RGC intrinsic excitability plays a crucial role in the effectiveness of transmitting electrical signals. Hence, assessing the RGC functional status in the degenerated retina is important. We first wanted to assess whether RGCs still generated APs. Using patch-clamp recording in RCS rats, our data revealed that all recorded RGCs retained their spiking ability until at least P90. Similarly, the spiking ability of RGCs with large somas were maintained in rd1 retinas[11]. A previous study on population activity using multielectrode arrays in P23H rats also supports our results, as a similar RGC stimulation success rate in these rats was observed compared with that in wild-type animals[7]. In contrast, a previous study in RCS rats showed that two-thirds of RGCs could not generate APs by a depolarizing pulse at P90[16]. The reason for this result was probably that these experiments were performed on retinal slices in which the retinal circuits and RGCs dendrites were largely damaged.

Secondly, we wanted to assess whether the level of RGC excitability decreases in degenerated retinas. Previous studies on stimulation thresholds in degenerated retinas were mainly performed using the extracellular stimulation method. Elevated stimulation thresholds were observed in numerous experiments using epiretinal or subretinal electrodes[17-21]. Among these experiments, epiretinal electrodes stimulate RGCs directly, and the stimulation threshold values are less affected by the remodelled circuitry in degenerated retinas[19,22]. However, they still are influenced by the position of the RGC relative to the electrode[23] and by the RGC density[18,23], among others. In a previous study, using a combination of whole-cell patch-clamp recording and extracellular stimulation in rd10 mice[45], distance variation between an external electrode and targeted RGC soma were avoided, and elevated extracellular stimulation thresholds were still observed compared to those in wild-type animals. Moreover, these phenomena were more pronounced in the low spontaneous spike rates group. In the present study, we observed a similar result from the perspective of intrinsic excitability, as RGCs with low spontaneous spike rates in RCS rats required more depolarizations to reach the APT than control rats. Furthermore, we identified the morphological types of RGCs, revealing that OFF RGCs, especially A2o cells, in RCS retinas require significantly higher currents to elicit an AP compared to these cells in control retinas.

In our study, the fact that more depolarizations were required to reach the APT in some RCS RGCs was mainly attributed to elevated ATPs, since RMPs in RCS RGCs were relatively stable compared with those in control RGCs. Sodium and potassium channels are known to be the two most important factors regulating RGC APs[35]. Because the initial rising phase from the RMP to the APT was mainly attributed to increased sodium conductance, the elevated APT values in RCS RGCs were most likely due to changes in sodium channels, including decreased channel density, alteration of their location along the membrane, and changes in their kinetic properties. In addition to the initial rising phase, other AP components were mainly attributed to sodium and potassium conductance. Since some potassium channel effects were removed by $Cs^+$ in our intracellular solution, the AP half width in our RGCs was wider than that achieved using an intracellular solution dominated by $K^+$[28,34]. Compared with control cells, RCS cells showed narrower APs; thus, we speculate that the kinetic properties of sodium and/or some potassium channels are altered in the RGCs of degenerated retinas. Quantifying and elucidating the kinetic properties of ion channels during the late stages of retinal degeneration are other areas requiring further investigation.

In addition to depolarization of the RMP toward the APT, the $R_m$ can also determine the amount of current required to generate an AP. In our study, $R_m$ values in C2o cells were significantly reduced, and $R_m$ values in other types of RGCs were slightly reduced in RCS rats. The $R_m$ is related to dendritic size, leak conductance and spontaneous synaptic input[2]. Since dendritic sizes remain stable in RCS RGCs, and since the steadiness of RMPs suggests that leak conductance are also stable in these cells, the decreases in $R_m$ were most likely due to stronger spontaneous synaptic inputs into RGCs in degenerated retinas, which has been reported in numerous studies. Specifically, inner retinal network oscillations have become a remarkable feature of retinal degeneration[11-15]. For the P90 RCS RGCs in our study, we also observed obvious oscillating activity in approximately 2/3 of the recorded cells,

and the C2o RCS: control ratio of the sum of the amplitudes of spontaneous EPSCs and IPSCs per second were 2.8 and 2.6 (data not shown).

Our results have several implications for RP therapeutic strategies, especially regarding electronic prostheses and optogenetics. First, the retention of dendritic morphologies in RGCs and their capability of generating APs during the late stages of retinal degeneration indicate that RGC population represent an attractive target for RP treatment. Second, intrinsic excitability was considerably decreased in some RGCs during the late stages of retinal degeneration; thus, degenerated retinas require higher stimulus intensities by electronic prostheses[5-7] and higher transgenic expression levels of light-sensitive cation channels, including Channerhodopsin2 (ChR2), melanopsin, and light-gated ionotropic glutamate receptor (LiGluR), into RGCs than normal retinas[8-10]. Furthermore, when optogenetic tools are applied to particular types of RGCs, the heterogeneity of the intrinsic excitability of various RGC types in the degenerated retina should also be considered.

**ACKNOWLEDGEMENTS**

**Authors' contributions:** Ren YM contributed to data collection and analyses, and manuscript writing. Weng CH contributed to data collection. Zhao CJ and Yin ZQ contributed to design and supervise the project as well as contributed to analyse data and revise the manuscript.

**Foundations:** Supported by the National Basic Research Program of China (973 Program, No.2013CB967002); the Military Key Program (No.BWS13C015); the Chongqing International Cooperation Key Projects (No. CSTC2013GJHZ10004).

**Conflicts of Interest: Ren YM,** None; **Weng CH,** None; **Zhao CJ,** None; **Yin ZQ,** None.

**REFERENCES**

1 Field GD, Chichilnisky EJ. Information processing in the primate retina: circuitry and coding. *Annu Rev Neurosci* 2007;30:1-30.

2 Wong RC, Cloherty SL, Ibbotson MR, O'Brien BJ. Intrinsic physiological properties of rat retinal ganglion cells with a comparative analysis. *J Neurophysiol* 2012;108(7):2008-2023.

3 Jones BW, Pfeiffer RL, Ferrell WD, Watt CB, Marmor M, Marc RE. Retinal remodeling in human retinitis pigmentosa. *Exp Eye Res* 2016;150: 149-165.

4 Jones BW, Kondo M, Terasaki H, Lin Y, McCall M, Marc RE. Retinal remodeling. *Jpn J Ophthalmol* 2012;56(4):289-306.

5 Humayun MS, Dorn JD, da Cruz L, Dagnelie G, Sahel JA, Stanga PE, Cideciyan AV, Duncan JL, Eliott D, Filley E, Ho AC, Santos A, Safran AB, Arditi A, Del Priore LV, Greenberg RJ. Interim results from the international trial of second Sight's visual prosthesis. *Ophthalmology* 2012;119(4):779-788.

6 da Cruz L, Coley BF, Dorn J, Merlini F, Filley E, Christopher P, Chen FK, Wuyyuru V, Sahel J, Stanga P, Humayun M, Greenberg RJ, Dagnelie G. The Argus II epiretinal prosthesis system allows letter and word reading and long-term function in patients with profound vision loss. *Br J Ophthalmol* 2013;97(5):632-636.

7 Sekirnjak C, Hulse C, Jepson LH, Hottowy P, Sher A, Dabrowski W, Litke AM, Chichilnisky EJ. Loss of responses to visual but not electrical stimulation in ganglion cells of rats with severe photoreceptor degeneration. *J Neurophysiol* 2009;102(6):3260-3269.

8 Bi A, Cui J, Ma YP, Olshevskaya E, Pu M, Dizhoor AM, Pan ZH. Ectopic expression of a microbial-type rhodopsin restores visual responses in mice with photoreceptor degeneration. *Neuron* 2006;50(1):23-33.

9 Caporale N, Kolstad KD, Lee T, Tochitsky I, Dalkara D, Trauner D, Kramer R, Dan Y, Isacoff EY, Flannery JG. LiGluR restores visual responses in rodent models of inherited blindness. *Mol Ther* 2011;19(7):1212-1219.

10 Lin B, Koizumi A, Tanaka N, Panda S, Masland RH. Restoration of visual function in retinal degeneration mice by ectopic expression of melanopsin. *Proc Natl Acad Sci U S A* 2008;105(41):16009-16014.

11 Margolis DJ, Newkirk G, Euler T, Detwiler PB. Functional stability of retinal ganglion cells after degeneration-induced changes in synaptic input. *J Neurosci* 2008;28(25):6526-6536.

12 Choi H, Zhang L, Cembrowski MS, Sabottke CF, Markowitz AL, Butts DA, Kath WL, Singer JH, Riecke H. Intrinsic bursting of AII amacrine cells underlies oscillations in the rd1 mouse retina. *J Neurophysiol* 2014;112(6):1491-1504.

13 Tu HY, Chen YJ, McQuiston AR, Chiao CC, Chen CK. A novel retinal oscillation mechanism in an autosomal dominant photoreceptor degeneration mouse model. *Front Cell Neurosci* 2015;9:513.

14 Biswas S, Haselier C, Mataruga A, Thumann G, Walter P, Müller F. Pharmacological analysis of intrinsic neuronal oscillations in rd10 retina. *PLoS One* 2014;9(6):e99075.

15 Trenholm S, Awatramani GB. Origins of spontaneous activity in the degenerating retina. *Front Cell Neurosci* 2015;9:277.

16 Chen Z, Song Y, Yao J, Weng C, Yin ZQ. Alterations of sodium and potassium channels of RGCs in RCS rat with the development of retinal degeneration. *J Mol Neurosci* 2013;51(3):976-985.

17 Ye JH, Goo YS. Comparison of voltage parameters for the stimulation of normal and degenerate retina. *Conf Proc IEEE Eng Med Biol Soc* 2007;2007:5783-5786.

18 Chan LL, Lee EJ, Humayun MS, Weiland JD. Both electrical stimulation thresholds and SMI-32-immunoreactive retinal ganglion cell density correlate with age in S334ter line 3 rat retina. *J Neurophysiol* 2011;105(6):2687-2697.

19 Margalit E, Babai N, Luo J, Thoreson WB. Inner and outer retinal mechanisms engaged by epiretinal stimulation in normal and rd mice. *Vis Neurosci* 2011;28(2):145-154.

20 Jensen RJ. Activation of ganglion cells in wild-type and P23H rat retinas with a small subretinal electrode. *Exp Eye Res* 2012;99:71-77.

21 Jensen RJ, Rizzo JF 3rd. Activation of retinal ganglion cells in wild-type and rd1 mice through electrical stimulation of the retinal neural network. *Vision Res* 2008;48(14):1562-1568.

22 O'Hearn TM, Sadda SR, Weiland JD, Maia M, Margalit E, Humayun MS. Electrical stimulation in normal and retinal degeneration (rd1) isolated mouse retina. *Vision Res* 2006;46(19):3198-3204.

23 Ahuja AK, Behrend MR. The Argus™ II retinal prosthesis: factors affecting patient selection for implantation. *Prog Retin Eye Res* 2013;36:1-23.

24 D'Cruz PM, Yasumura D, Weir J, Matthes MT, Abderrahim H, LaVail MM, Vollrath D. Mutation of the receptor tyrosine kinase gene Mertk in the retinal dystrophic RCS rat. *Hum Mol Genet* 2000;9(4):645-651.

25 Liu X, Zhang Y, He Y, Zhao J, Su G. Progress in histopathologic and pathogenetic research in a retinitis pigmentosa model. *Histol Histopathol* 2015;30(7):771-779.

26 Muñoz F, Fuentealba P. Dynamics of action potential initiation in the GABAergic thalamic reticular nucleus in vivo. *PLoS One* 2012;7(1): e30154.

27 Schmidt TM, Kofuji P. An isolated retinal preparation to record light response from genetically labeled retinal ganglion cells. *J Vis Exp* 2011;26(47):2367-2370.

28 Qu J, Myhr KL. The development of intrinsic excitability in mouse retinal ganglion cells. *Dev Neurobiol* 2008;68(9):1196-1212.

29 Sun W, Li N, He S. Large-scale morophological survey of rat retinal ganglion cells. *Vis Neurosci* 2002;19(4):483-493.

30 Sun W, Li N, He S. Large-scale morphological survey of mouse retinal ganglion cells. *J Comp Neurol* 2002;451(2):115-126.

31 Kostal L, Lansky P, Rospars JP. Neuronal coding and spiking randomness. *Eur J Neurosci* 2007;26(10):2693-2701.

32 Yee CW, Toychiev AH, Ivanova E, Sagdullaev BT. Aberrant synaptic input to retinal ganglion cells varies with morphology in a mouse model of retinal degeneration. *J Comp Neurol* 2014;522(18):4085-4099.

33 Schiller PH. Parallel information processing channels created in the retina. *Proc Natl Acad Sci U S A* 2010;107(40):17087-17094.

34 Wang GY, Ratto G, Bisti S, Chalupa LM. Functional development of intrinsic properties in ganglion cells of the mammalian retina. *J Neurophysiol* 1997;78(6):2895-2903.

35 Sernagor E, Eglen SJ, Wong RO. Development of retinal ganglion cell structure and function. *Prog Retin Eye Res* 2001;20(2):139-174.

36 Usrey WM, Reppas JB, Reid RC. Paired-spike interactions and synaptic efficacy of retinal inputs to the thalamus. *Nature* 1998;395(6700): 384-387.

37 Kim IJ, Zhang Y, Yamagata M, Meister M, Sanes JR. Molecular identification of a retinal cell type that responds to upward motion. *Nature* 2008;452(7186):478-482.

38 Lin B, Peng EB. Retinal ganglion cells are resistant to photoreceptor loss in retinal degeneration. *PLoS One* 2013;8(6):e68084.

39 O'Brien EE, Greferath U, Fletcher EL. The effect of photoreceptor degeneration on ganglion cell morphology. *J Comp Neurol* 2014;522(5): 1155-1170.

40 Mazzoni F, Novelli E, Strettoi E. Retinal ganglion cells survive and maintain normal dendritic morphology in a mouse model of inherited photoreceptor degeneration. *J Neurosci* 2008;28(52):14282-14292.

41 Chang B, Hawes NL, Pardue MT, German AM, Hurd RE, Davisson MT, Nusinowitz S, Rengarajan K, Boyd AP, Sidney SS, Phillips MJ, Stewart RE, Chaudhury R, Nickerson JM, Heckenlively JR, Boatright JH. Two mouse retinal degenerations caused by missense mutations in the beta-subunit of rod cGMP phosphodiesterase gene. *Vision Res* 2007;47(5): 624-633.

42 Kalloniatis M, Nivison-Smith L, Chua J, Acosta ML, Fletcher EL. Using the rd1 mouse to understand functional and anatomical retinal remodelling and treatment implications in retinitis pigmentosa: a review. *Exp Eye Res* 2016;150:106-121.

43 Villegas-Pérez MP, Lawrence JM, Vidal-Sanz M, Lavail MM, Lund RD. Ganglion cell loss in RCS rat retina: a result of compression of axons by contracting intraretinal vessels linked to the pigment epithelium. *J Comp Neurol* 1998;392(1):58-77.

44 Pavlidis M, Fischer D, Thanos S. Photoreceptor degeneration in the RCS rat attenuates dendritic transport and axonal regeneration of ganglion cells. *Invest Ophthalmol Vis Sci* 2000;41(8):2318-2328.

45 Cho A, Ratliff C, Sampath A, Weiland J. Changes in ganglion cell physiology during retinal degeneration influence excitability by prosthetic electrodes. *J Neural Eng* 2016;13(2):025001.